Polymer Bulletin (2021) 78:4987–5001
https://doi.org/10.1007/s00289-020-03350-w

ORIGINAL PAPER

Influence of pore size and isosteric heat of adsorption of some metal–organic frameworks on the volumetric and gravimetric adsorption capacities of hydrogen at room temperature

Gustave Assoualaye[1] · Noël Djongyang[1]

Received: 28 January 2020 / Revised: 16 June 2020 / Accepted: 17 August 2020 /
Published online: 27 August 2020

Abstract

Metal–organic frameworks (MOFs) are presented as potential candidates to meet the challenge of storing hydrogen at room temperature. However, few hydrogen adsorbents balance high volumetric and gravimetric capacities. In this work, a series of ten MOFs of different topologies were selected to determine on the one hand the characteristics of MOFs capable of balancing the volumetric and gravimetric adsorption capacities of hydrogen at room temperature and on the other hand a correlation between the adsorption properties and the structure of MOF. The influence of characteristics such as free volume, pore diameter, and isosteric heat of adsorption on optimal adsorption at room temperature was evaluated. The results showed that the absolute gravimetric absorption capacity is well correlated with the free volume of the pores. The gravimetric and volumetric capacities of hydrogen absorbents can be balanced and increased by using materials that provide high isosteric heat of absorption. Small pore materials provide high isosteric adsorption heat but adsorb less due to the low free volume.

Introduction

Climate change and energy security are the two most important issues facing the world. The first requires a strong acceleration of innovation in energy technologies and non-carbon processes [1], and the second caused by the depletion of fossil resources leads massively to the introduction of intermittent renewable energy [2, 3]. Among the different energy sources, hydrogen has received a lot of attention because it has many fascinating benefits, including non-toxicity, abundance, and

✉ Noël Djongyang
noeldjongyang@gmail.com

[1] Department of Renewable Energy, National Advanced School of Engineering of Maroua, University of Maroua, PO Box 46, Maroua, Cameroon

easy preparation [4–7]. It would thus constitute an opportunity to develop innovative systems integrating an ecological dimension that weighs more and more in individual and societal choices [8].

Although globally recognized as a high-potential energy carrier, its large-scale use has faced numerous production [9] and storage challenges [10, 11]. However, in recent years, its production has posed no problem because several environmentally friendly methods have emerged, like electrolysis associated with solar, wind, hydroelectric, or biomass energy, which are renewable sources allowing a large production of hydrogen without pollution [1]. It can also be produced by biological processes [4]. Yet, its safe and efficient storage remains very expensive for a wide application.

Several techniques exist for the storage of hydrogen [12]. But the two conceptually simple methods are compression under a pressure of 700 bars and liquefaction at a temperature of 20 K [13]. However, the pressurized gas tank presents key problems in the design and sealing of materials; moreover, reaching the desired pressure requires more than 10% of the stored energy [14, 15]. Also, in the cryogenic method, large amounts of energy are lost during the liquefaction and evaporation processes. Consequently, these two methods consume a lot of energy and are not economically the most indicated [15, 16]. To overcome these various difficulties, the use of adsorbent materials is a method which fascinates researchers in this field.

Among all porous materials, metal–organic frameworks (MOFs) are the best candidates for adsorption of H2 because they are made up of light atoms and are very porous. In addition, they hold the best hydrogen storage records these days [2, 3, 6, 17–19].

Some MOFs show the satisfactory results when they operate at cryogenic temperatures [19]. However, for operation at 77 K, additional energy and equipment are required to keep the tanks at a temperature below that of the environment [6]. In addition, there is also the problem of heat transfer [20]; this is why the adsorption of hydrogen at ambient temperature and pressure would be ideal [8]. But at room temperature, their storage capacity becomes low, due to the weak MOF-H_2 interactions [8, 19]. It is, therefore, necessary to find materials which can function under these conditions, that is to say, which can respond to practical application requirements set by the United States Department of Energy (DOE) in 2020. (5.5wt.% of gravimetric density and 40 g. L^{-1} of volumetric density at an operating temperature between 233 and 333 K and at a pressure below 12 atm) [20, 21].

Some work has already been done on the storage of hydrogen at moderate temperatures and pressures. Hirscher et al. [22] demonstrated that the properties of materials such as the surface, composition, and size of the pores can influence the storage capacity and that it would, therefore, be necessary to understand the correlation between the adsorption properties and the structure of MOFs to improve hydrogen storage. Njikamp et al. [23] found that carbon and low pore volume zeolites are not good candidates for storing hydrogen under its recommended conditions. Frost and Snurr [24] suggested that a hydrogen storage capacity of 9 wt.% and 30 g. L^{-1}could be reached with MOFs which can provide isosteric heat of 15 kJ. Mol^{-1} while maintaining a free volume of 2.5 cm^3. g^{-1} and a vacuum fraction of 0.85. Bhatia and Myers [25] have determined operating conditions of 131 K and 1.5 to 100 bar for a microporous material having an enthalpy of adsorption equal to 6 kJ. Mol^{-1}. Thornton et al. [26] found that

characteristics that maximize optimal storage capacities at room temperature include pores of about 6 Å in diameter and vacuum fractions of 0.1. The results have been corroborated with the work of Hao Li et al. [6], who find that the MOFs–H2 interaction force can be refined by the size and shape of the pores.

In this work, we study the influences of several characteristics of the MOF for optimal adsorption of the gravimetric and volumetric capacities coupled, because few hydrogen adsorbents balance high usable volumetric and gravimetric capacities. These characteristics are the gravimetric and volumetric surface of the MOF, the volume of the pores, the void fraction, the diameter of the pores, the heat of isosteric adsorption, the types of construction networks and the influence of the introduction of metal ions into the SBUs of MOFs. However, the large number of existing MOFs pushes researchers to turn to computer simulations to limit the expenses linked to the experiments. This will also allow a custom design of these hydrogen adsorbent materials.

Frost and Snurr studied the effects of specific surface area, free volume and heat of adsorption on the absorption of H2 by GCMC simulations over a wide pressure range at 298 K, but this study was not carried out than on a series of MOFs belonging to a single family (IRMOF). However, in our work, we used ten MOFs from several families. These adsorbent materials have several topologies and are built according to two main objectives. The first is to increase the area and volume of the pores using ligand elongation or mixed ligand systems. And second, in order to increase the isosteric heat of hydrogen adsorption, MOFs are designed with: open metal sites, the introduction of cations generating a large electrostatic field in the cavities, doping with metal ions, the manufacture of metal nanoparticles, and the functionalization of ligands.

The first materials are the MOF which best balances the volumetric and gravimetric adsorption capacity of hydrogen at 77 K, like IRMOF-1 which is presented as the reference MOF by the Center of Excellence for Engineering hydrogen storage (HSECoE) [27, 28]. According to the work of Ahmed et al. [29, 30], IRMOF-20, PCN-610 / NU-100 [31], and SNU-70 [32] had higher capacities than those of IRMOF-1. Cu-BTC [33] is the type of open metallic MOF, designed to increase the attraction between MOF and the hydrogen molecule. The elongation of the ligands in the structure of MOF-177 and MOF-200 increases their specific surface [34]. Finally, MOF-74, ZnMOF-74, and MgMOF-74 [35] were chosen to evaluate the influence of the introduction of metal ions into MOF. For each MOF, the different characteristics such as the pore volume, the largest cavity diameters, the specific surface, the helium vacuum fractions, and the isosteric heats of adsorption are determined and are shown in Table 1.

Simulation methods

In the simulations, linkage interactions are neglected because we have assumed rigid molecules. In this case, there are only intermolecular interactions between unbound atoms, which are modeled via a Lennard–Jones potential (LJ) + Coulomb potential [36] represented by Eq. (1).

Table 1 Properties of the MOF materials studies

Frameworks	Gravimetric surface area ($m^2.g^{-1}$)	Volumetric surface area ($m^2.cm^{-3}$)	Pore volume $cm^{-3}.g^{-1}$	Void fraction ($\dot{A}$)	Diameter pores	Qst kJ. mol^{-1}
IRMOF-1	3563	2172	1.36	0.80	15.01	4.68
IRMOF-20	3137	2057	1.54	0.96	17.28	5.75
HKUST-1	2340	2057	0.82	0.74	3.19	4.74
MOF-177	4849	2069	1.95	0.83	11.17	4.75
MOF-200	6195	1331	4.22	0.91	17.97	4.01
MOF-74	775	1346	0.27	0.39	7.04	6.38
ZnMOF-74	1341	1581	0.56	0.65	11.91	5.77
MgMOF-74	1784	1576	0.74	0.65	11.86	5.57
SNU-70	4227	1955	1.4	0.86	17.98	4.88
PCN-610/ NU-100	5718	1725	2.90	0.87	13.81	4.42

$$U_T = \sum_{i\langle j} 4\varepsilon_{ij}.[(\frac{\sigma_{ij}}{r_{ij}})^{12} - (\frac{\sigma_{ij}}{r_{ij}})^{6}] + \sum_{i\rangle j} \frac{q_i q_j}{4\pi\varepsilon_0 r_{ij}} \quad (1)$$

where ε is the depth of the potential well, σ is the finite distance at which the inter particle potential is zero, r is the distance between the particles, andq_1 and q_2 are the positive or negative magnitudes of the charges.

The hydrogen molecules have been modeled according to the Darkrim–Levesque model [37]. The LJ parameters for the MOF atoms were assigned according to the Universal Force Field (UFF) [38] and Dreiding [39]. A limit value of 12 Å was used for all LJ interactions, and Ewald summations were used to calculate Coulomb interactions. Equations (2) and (3) present the Lorentz–Berthelot [40] mixing rules used to determine the LJ parameters for the interactions between atoms.

$$\varepsilon_{ij} = \sqrt{\varepsilon_{ii}.\varepsilon_{jj}} \quad (2)$$

$$\sigma_{ij} = \frac{\sigma_{ii} + \sigma_{jj}}{2} \quad (3)$$

Adsorption simulations were performed in a single cell using Grand Canonical Monte Carlo simulations (GCMC) using the RASPA code [41]. To calculate the ensemble averages, in each cycle, an average of N displacements was made, where N is the number of H_2 molecules in the system. Translation, rotation, insertion, deletion, and reintegration movements were used with equal probability.

The geometric area was calculated by the Monte Carlo method using a probe of 2.958 Å equal to the diameter of the hydrogen atom. The void fraction, which is the void of a structure divided by the total volume, is measured using helium, since the helium almost does not adsorb at room temperature. The isosteric heats

of H_2 adsorption shown are low coverage data, calculated at a temperature of 298 K and at a pressure of 0.5 Bar.

For the description of the MOFs, characteristics such as pore volume, largest cavity diameter, and specific surface area were calculated using Zoe++[42], while helium vacuum fractions and adsorption heats were determined using RASPA.

Results and discussions

Figure 1 compares the results obtained in this work to those of Frost and Snurr [24]. Figure 1a shows the excess adsorption of H_2 in IRMOF-1 at 298 K, and Fig. 1b shows the results of excess adsorption in Cu-BTC or HKUST-1 at 298 K. Simulations were performed over a pressure range from 1 to 100 bar. The results were compared to those of Frost and Snurr because they used a relatively simple model similar to that used in the current work and obtained the acceptable results. However, we can observe a slight difference (0.1–0.5) during the increased pressures. This could be explained by the fact that our model takes a limit value of 12 Å for all interactions of Lennard–Jones J compared to the 12,8 Å used in their work. Although these results are significantly lower than the experimental results which were high (up to 1*wt.*% at 20 bar) [43], it was shown that these experimental results were very likely to be contaminated by the presence of another gas.

Figure 2 shows the gravimetric hydrogen adsorption capacities of the different MOFs studied. This capacity is given by the ratio between the mass of hydrogen stored and that of the MOF loaded with hydrogen. we note that the MOF-200 provides the greatest absolute gravimetric capacity at 298 K; it adsorbs up to 3.7 wt.% H_2 at 100 bar, followed by the PCN-610 which has a capacity of 2.8 wt.% under the same conditions. The MOF-177 having the same topology as the MOF-200 has a capacity of 1.9 wt.% SNU-70 has a capacity of 1.77 wt.%; IRMOF-20 adsorbs 1.55 wt.%, and IRMOF-1 stores 1.3 wt.% H_2. It is observed that the curves of the hydrogen adsorption isotherms at 298 K obtained for the different materials are linear pressure functions like that found in the literature [43]. This

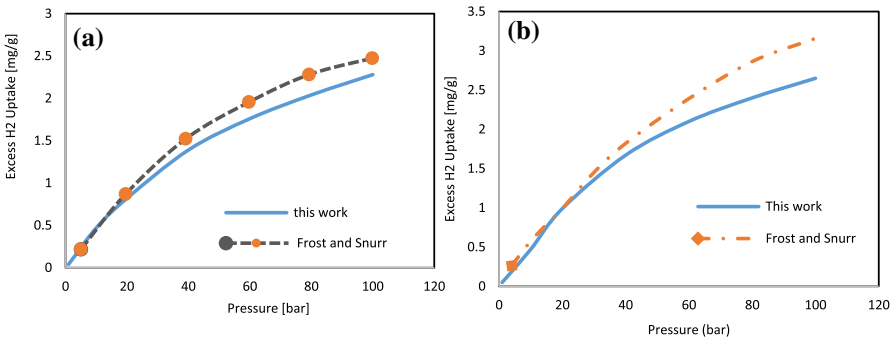

Fig. 1 **a** Simulated adsorption isotherms for IRMOF-1 at 298 K and **b** simulated adsorption isotherms for Cu-BTC at 298 K

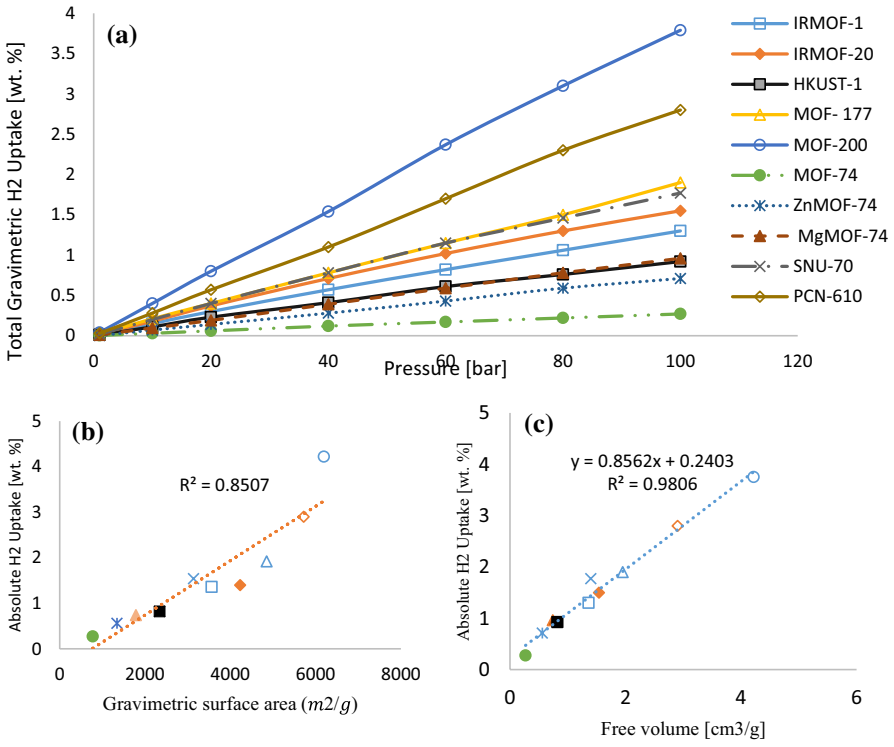

Fig. 2 **a** Absolute gravimetric hydrogen adsorption in ten MOF materials at 298 K, **b** correlation of the absolute gravimetric H_2 adsorption at 100 bar and 298 K gravimetric surface area and **c** correlation of the absolute gravimetric H_2 adsorption at 100 bar and 298 K with free volume

is justified by the fact that no saturation occurs in the pressure range studied and that the layer of hydrogen adsorbed on the surface of the MOF is very dilute. The difference between the performances of MOFs comes first from the specific surface. As the specific surface is the total surface, it comprises on the one hand the geometric or "exterior" area, and on the other hand, the "interior" surface formed by the walls of the capillaries, pores, or crevices of the solid. Then, the MOF having the largest surface will be able to adsorb a large quantity of hydrogen because adsorption is a surface phenomenon that occurs during contact between a gas or a liquid with a solid. This is why Fig. 2b shows that the correlation between the absolute gravimetric adsorption and the gravimetric surface of the different MOFs is 0.8507. From the characteristics of the MOFs calculated in Table 1, we observe that the surface mainly increases with the diameters of the pores. However, as the MOF-177 has pores with diameters equal to 11.17 A and shows a greater specific surface area than the ZnMOF-74 or MgMOF-74 which have pores with diameters 11.91 and 11.86 A, respectively, we can also affirm that the topology of MOFs is a factor which also influences their gravimetric capacity of hydrogen adsorption.

As we said above, the surface called here "interior" which is formed by the walls of capillaries, pores, or crevices can certainly contain small cavities inaccessible to the molecules to be adsorbed. To assess their influence, we calculated the pore volume with a probe size equal to that of hydrogen which is 2.958 A. The results of R^2 in Fig. 2c for the absolute gravimetric adsorption show a correlation with the free volume greater than that obtained with the gravimetric surface in Fig. 2b. We can then say that the materials with the largest free volume available will contain the most hydrogen. This is why, for the design of a material capable of overcoming the challenges of gravimetric adsorption, it is necessary to increase the specific surface of the MOFs and to eliminate the cavities of size smaller than the diameter of the hydrogen because they will not allow its penetration.

The isosteric adsorption heat of the Materials can be increased by decreasing the pore size. This is what one can observe in Fig. 3. MOF-74 has pore sizes of 7 Å and provides an isosteric heat of 6.38 kJ. mol^{-1} which is the largest of all MOF studied. We have also noted that the introduction into this material of the metal ions Mg (II) and Zn (II) does not increase the isosteric heat of adsorption but earlier increases the pore diameters which are 11.86 and 11.91 Å for MgMOF-74 and ZnMOF-74, respectively, for an isosteric heat of 5.57 and 5.77 kJ. mol^{-1}, but comparing to materials with the same pore diameters, such as MOF-177, MgMOF-74, and ZnMOF-74 are much better. We can say that MOFs doped with metal ions provide more adsorption heat than MOFs with the same characteristics. The main reason why the MOF-74 has the smallest gravimetric capacity is that it has small pores that give it a small free volume. Pore size can affect the interaction between hydrogen molecules and porous solids. The materials containing small pores and high curvature walls interact more strongly with hydrogen molecules than large-pore materials. This provides solid evidence that the smaller the pores, the stronger the interactions between MOF and H_2.

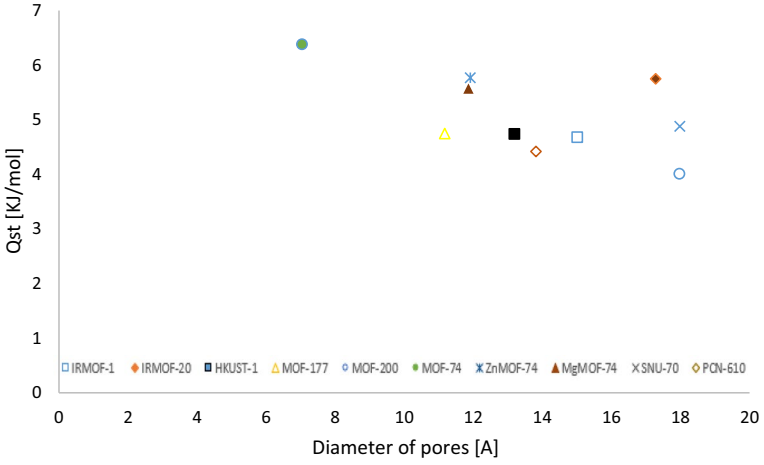

Fig. 3 Correlation of Qst with pore diameter for the ten MOFs

The study of excess adsorption is crucial to understanding the physical adsorption of materials. Absolute adsorption is the sum of excess adsorption (molecules that attach to the surface through Van der Waal interactions) and the capacity that resides in the pores. The reason why we have an almost linear correlation with the free volume, to observe in Fig. 2c, comes from the fact that the interactions are very weak at ambient temperature. The excess of adsorptions presents a complex correlation. We can notice that the excess is related to the accessible or available surface because, for a large area, there will also be many hydrogen molecules that can be adsorbed. In Fig. 4, the MOF-200 exhibits the largest PCN-610 over-capacity survivability that provides 0.42 wt.% capacitances and 0.41 wt.% at 100 bar and 298 K, because they have the biggest surfaces. However, we observe that they have curves that already reach their saturation at 100 bar, unlike MOFs that have higher isosteric heat. Although not having the highest performance over this range of pressures, the MgMOF-74 and ZnMOF-74 provide nearly linear curves that prove that for slightly greater pressures these materials will give the greatest excess capacity.

Conceptually, the difference between absolute values and excessive values can be considered as a gas in its ambient state, that is to say a gas that would exist in the pores even if the material did not provide interaction energy. As the density of ambient H_2 will be the same in all materials, it is the free volume that determines the amount of ambient H_2 that exists per mass of material.

The MOF-filled tank required to store a certain amount of the hydrogen should be neither too heavy nor too large to meet certain requirements in the current fashion of vehicle design. However, these tanks must also have reasonable autonomy. To determine the size and mass of these tanks, the volumetric and gravimetric capacities are key factors. Yet, as we observe in Fig. 5, in which we have shown the volumetric capacity curves of the different materials over a pressure range from 1 to 100 bar at 298 K, the MOF-200 which has the highest gravimetric

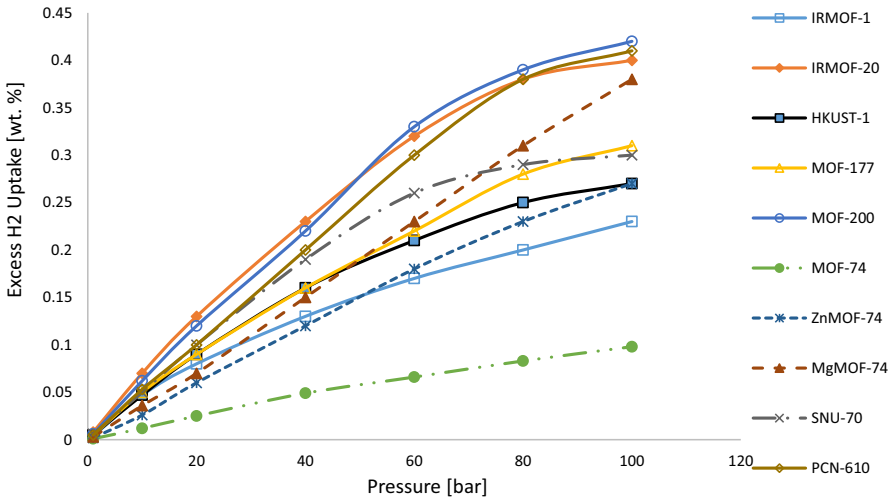

Fig. 4 Excess hydrogen adsorption in ten MOF materials at 298 K

capacity provides a volumetric capacity of 8.89 gH_2. L^{-1} which is the lowest. We note then that the objectives of individual maximization of volumetric and gravimetric hydrogen adsorption charges MOF are incompatible, which is related to the ref. [44]. The poor performance of materials in general is due to the low density of hydrogen at room temperature. As can be seen in Fig. 6a, materials with large specific surface areas have low volumetric capacities. MgMOF-74, ZnMOF-74, and SNU-70 are the three materials that provide the largest volumetric capacities that are 13.02, 12.69, and 12.64 gH_2. L^{-1}, respectively, at a temperature of 298 K and a pressure of 100 bar.

Some work has found that the density of H_2 in the H2 pores depends on the size of the pores. We note in Fig. 6b that the SNU-70 has pores approximately 17.98 Å in diameter which are largely above the other MOFs studied but have a capacity close to MgMOF-74 and ZnMOF-74. We note that the study of the density of H2 in the pores or the free volume makes it possible to examine more clearly the effects of the characteristics on the adsorption of the H2 in the MOFs, because the quantity of hydrogen in a volume should be the same then the difference that we notice would be due to the excess of adsorption that is to say the quantity which is fixed on the surface. Intuitively, we can already see that at low pressure the excess is correlated with the accessible surface and that at high pressures, MOF–H2 interactions control this capacity.

Because a material with large pores can provide strong interaction energies near the walls but will have more space farther from the walls where the adsorbate molecules have little attraction on the surface of the material, in Fig. 6c, we can notice that there is a slight correlation with isosteric adsorption heat. But as the MOF-74 has a very small surface, despite its high isosteric heat it has a low capacity.

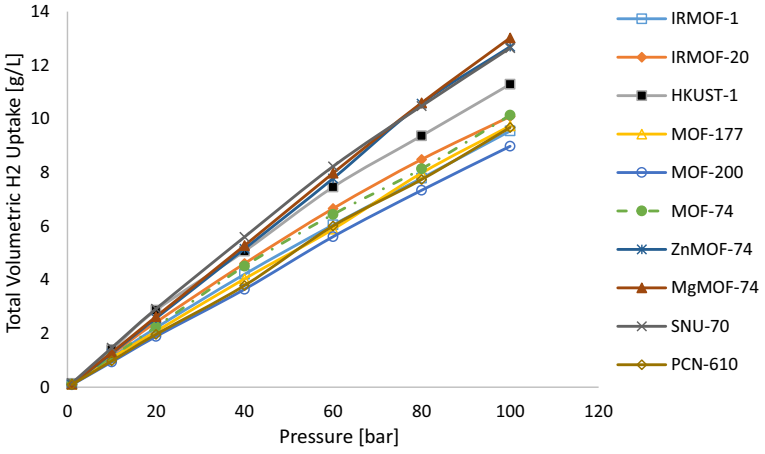

Fig. 5 Absolute volumetric hydrogen adsorption in ten MOF materials at 298 K

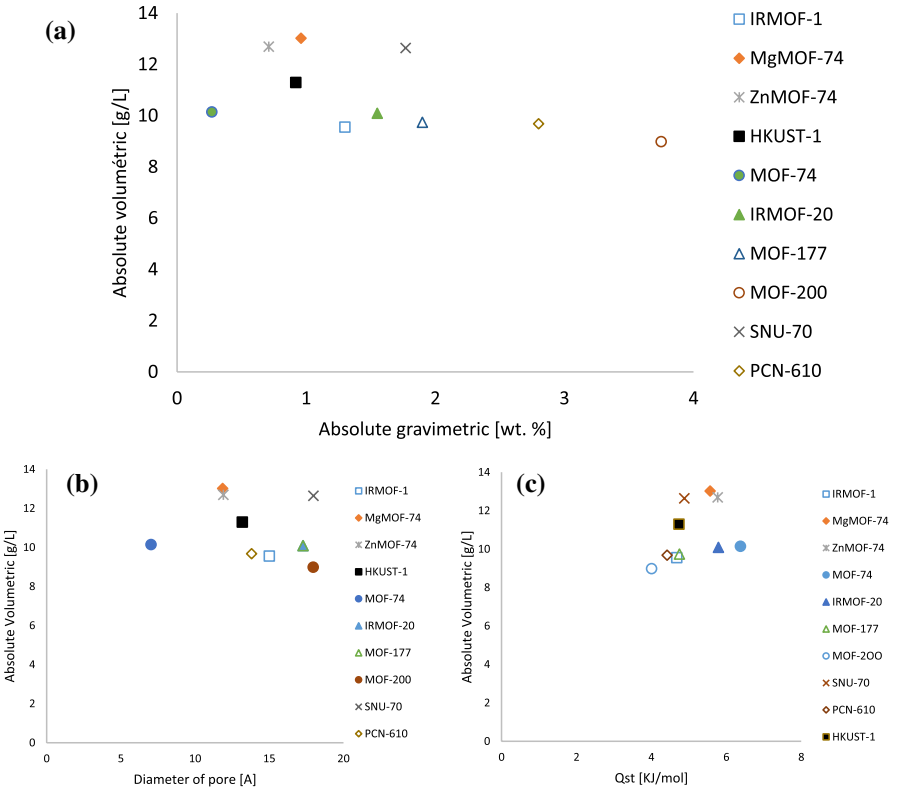

Fig. 6 **a** Correlation of the absolute volumetric H2 adsorption at 100 bar and 298 K with absolute gravimetric H2 adsorption in ten MOF, **b** correlation of the absolute volumetric H2 adsorption at 100 bar and 298 K pores diameters of ten MOF, and **c** correlation of absolute volumetric H2 adsorption at 100 bar and 298 K with adsorption isosteric heat in ten MOF

Figure 4 provides a useful relationship between the gravimetric hydrogen capacity in the MOFs to study and the free volume at 100 bar and 298 K. A line fitted to their data gives us the empirical equation:

$$N_{\text{abs}} = 0.86 \times V_l + 0.24 \tag{4}$$

where N_{abs} is the absolute capacity in wt. % and V_l the free volume by mass.

From this relationship, we vary the free volume by mass for the ten MOF to find a correlation between gravimetric and volumetric capacity. We find in Fig. 7 that it is difficult for a material to balance high volumetric and gravimetric capacity with low isosteric adsorption scale.

Using the empirical Frost–Snurr equation [24] linking the absolute density of hydrogen in the pores and the low charge isosteric heat is given by:

$$\rho_{\text{abs}} = 2,38 \times q_{\text{st}} + 1,79 \tag{5}$$

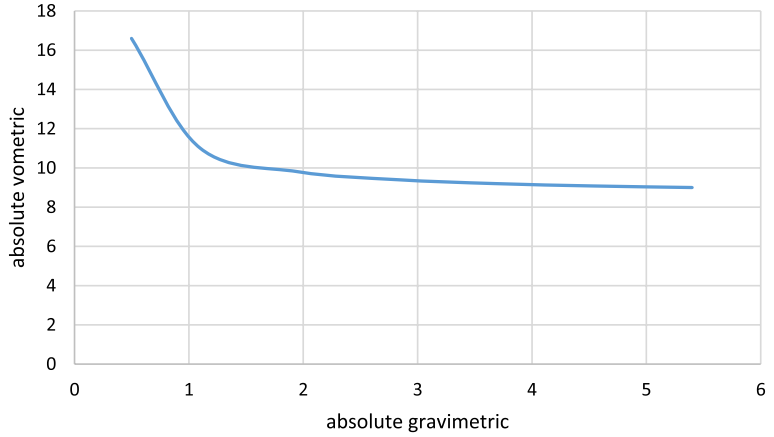

Fig. 7 Equilibrium between the gravimetric and volumetric adsorption capacities in the MOF at 298 K and 100

where ρ_{abs} is the absolute density of hydrogen in the pores and q_{st} isosteric low-load adsorption heat.

As this empirical equation has been adjusted to give the IRMOF-1 and Cu-BTC, we have chosen to use these two materials. We have calculated the adsorption capacity of these MOFs for two isosteric adsorption heat. As shown in Fig. 8, the first points showing weak capabilities were calculated with their natural isosteric heat. The higher points were calculated for an adsorption isosteric heat of 15 kJ. mol^{-1}. As already predicted Frost, we notice that they give the results very close to the goal. We also want to emphasize that the balance between gravimetric and volumetric capacity seems to be perfect for this value of Qst.

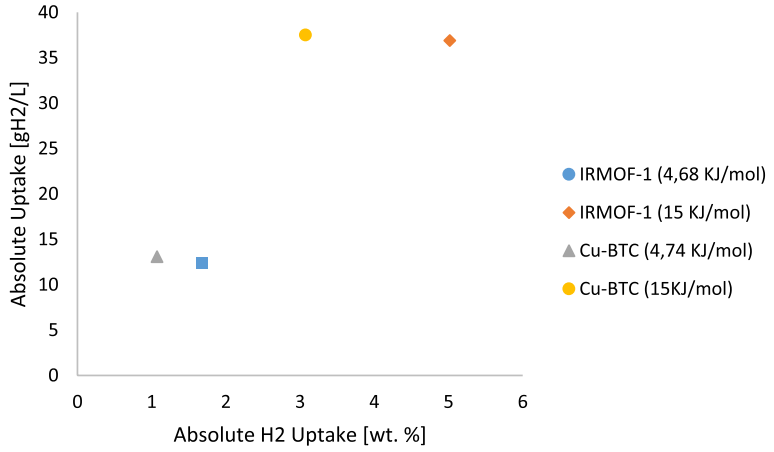

Fig. 8 Influence of isosteric adsorption heat on the balance between gravimetric and volumetric adsorption capacities in IRMOF-1 and Cu-BTC

Figure 9a and b shows the usable capacities of the different materials studied in this work. The useful capacity is defined as the difference in total absorption at 100 bar (filled tank) and 5 bar (empty tank) [29]. As shown in Fig. 9a, we note that the usable volumetric capacity varies from 8.5 to 12.3 $gH_2.L^{-1}$ and MgMOF-74 is the material which obtains the highest performances. Figure 9b also shows that the usable gravimetric capacities vary from 0.25 to 3.59% by weight. The MOF-200 has the highest usable gravimetric capacity. We note that the balance of usable adsorption capacities of MOFs at room temperature is different from that obtained at 77 k [29]. The usable gravimetric capacities of four materials calculated here always follow the order of the capacities measured at 77 k, PCN-610 (2.66 wt%), SNU-70 (1.67 wt%), IRMOF-20(1.45 wt%), and IRMOF-1(1.22 wt%). However, for the usable volumetric capacity, the order differs from that measured at low temperature. The PCN-610 which has the largest capacity at 77 k obtains at 298 k a capacity (9.17 $gH_2.\ L^{-1}$) lower than IRMOF-20 (9.42 $gH_2.\ L^{-1}$). At low temperature, the

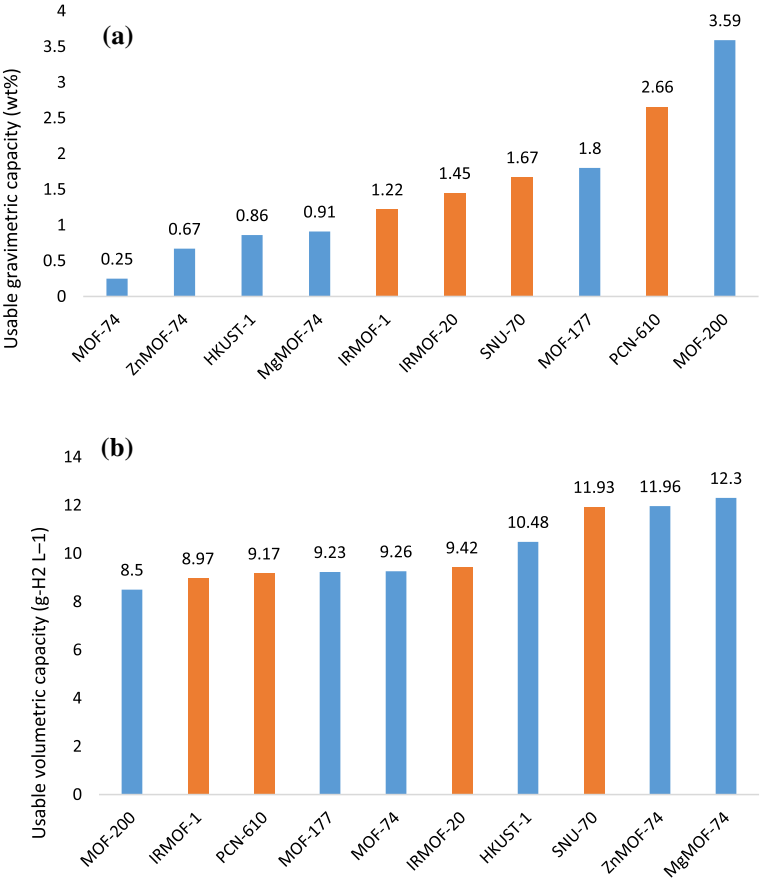

Fig. 9 Usable capacities of hydrogen stored by MOFs. **a** Volumetric basis and **b** gravimetric basis. Capacities are calculated at a temperature of 298 k and with a pressure variation of 100 and 5 bars

materials which have the greatest usable volumetric capacities also exhibit the greatest gravimetric capacities. we can, therefore, conclude here that the properties that some MOFs have for balancing the usable gravimetric and volumetric capacities can change with temperature.

MOFs that can store hydrogen at room temperature must have large pores to increase free volume. To increase the excess capacity, we have found that it takes a large area and increase the isosteric heat of adsorption. The functionalization of the surface of the host material with a transition metal attracting hydrogen by Kubas interactions will improve the physisorption energy of hydrogen by MOF.

Conclusion

We evaluated the influence of accessible surface area, pore size, and isosteric heat for a series of ten MOFs for adsorption at room temperature over a pressure range of 1 to 100 bar. Our results showed that the absolute gravimetric adsorption capacity of all materials is well correlated with the free volume of the pores. The excess has a somewhat more complex correlation; it is correlated with the accessible surface, but for pressures above 100 bar the materials providing isosteric heat of higher adsorption will adsorb more hydrogen. MOFs with a large gravimetric capacity give a low volumetric capacity. So, to achieve the objectives set for the storage of hydrogen must be designed MOF with high isosteric heat. Small pores increase the adsorbent–adsorbate interaction but give a low absolute capacity. To increase the isosteric heat of MOF, the functionalization of the surface of the host material with a transition metal seems to be the best option.

Acknowledgements The authors are thankful to The Cambridge Crystallographic Data Center (CCDC) for the material files graciously made available to us through Dr Yves Alain Mbiangué and to the developers of the RASPA particularly Dr Randall Snurr and Zeo ++ software with which we made simulations.

Compliance with ethical standards

Conflict of interest The authors declare that there is no conflict of interest in regard with this work.

References

1. Bercegol Hervé, Didierjean Sophie, Étienne Mathieu et al., « De nouvelles technologies de l'énergie en rupture ? », Annales des Mines–Responsabilité et environnement, 2019/3 (N° 95), p. 62–66. https://www.cairn.info/revue-responsabilite-et-environnement-2019–3-page-62.htm. Accessed 20 Nov 2019
2. Basdogan Y, Keskin S (2015) Simulation and modelling of MOFs for hydrogen storage. CrystEngComm 17(2):261–275. https://doi.org/10.1039/c4ce01711k
3. Prachi Prabhukhot R, Wagh MM, Gangal Aneesh C (2016) A review on solid state hydrogen storage material. Adv Energy Power 4(2):11–22. https://doi.org/10.13189/aep.2016.040202
4. Li H, Wang K, Sun Y, Lollar CT, Li J, Zhou H-C (2018) Recent advances in gas storage and separation using metal–organic frameworks. Mater Today 21(2):108–121. https://doi.org/10.1016/j.mattod.2017.07.006

5. Ghiyasiyan-Arani M, Salavati-Niasari M (2018) Effect of Li2CoMn3O8 Nanostructures synthesized by a combustion method on montmorillonite K10 as a potential hydrogen storage material. J Phys Chem C 122(29):16498–16509. https://doi.org/10.1021/acs.jpcc.8b02617
6. Zohuri B (2018) Hydrogen: driving renewable energy. Hydrogen Energy. https://doi.org/10.1007/978-3-319-93461-7_5
7. Brangier E, Vivian R, Bornet C (2019) Méthodes d'ergonomie prospective appliquées à l'identification de besoins pour des systèmes d'énergie à base d'hydrogène : étude exploratoire. Psychol Française. https://doi.org/10.1016/j.psfr.2019.02.002
8. García-Holley P, Schweitzer B, Islamoglu T, Liu Y, Lin L, Rodriguez S, Farha OK (2018) Benchmark study of hydrogen storage in metal-organic frameworks under temperature and pressure swing conditions. ACS Energy Letters 3(3):748–754. https://doi.org/10.1021/acsenergylett.8b00154
9. Kothari R, Buddhi D, Sawhney RL (2008) Comparison of environmental and economic aspects of various hydrogen production methods. Renew Sustain Energy Rev 12(2):553–563. https://doi.org/10.1016/j.rser.2006.07
10. A. Kamaruddin, G. Postole, A. Auroux, B. Galey. Etude de l'impact de la nanostructuration de MgH2 sur les propriétés de stockage de l'hydrogène. Journée de Printemps de la section Rhône-Alpes de la SCF, Jun 2019, Saint-Martin d'Hères, France. ⟨hal-02174523⟩
11. Menia S, Nouicer I, Bakouri Y, M'raoui A, Tebibel H, Khellaf A (2019) Production d'hydrogène par procédés biologiques. Oil Gas Sci Technol Rev IFP Energ Nouvelles 74:34. https://doi.org/10.2516/ogst/2018099
12. Gholami T, Salavati-Niasari M, Salehabadi A, Amiri M, Shabani-Nooshabadi M, Rezaie M (2018) Electrochemical hydrogen storage properties of NiAl 2 O 4 /NiO nanostructures using TiO 2, SiO 2 and graphene by auto-combustion method using green tea extract. Renew Energy 115:199–207. https://doi.org/10.1016/j.renene.2017.08.037
13. Jepsen J, Capurso G, Puszkiel J, Busch N, Werner T, Milanese C, Klassen T (2019) Effect of the process parameters on the energy transfer during the synthesis of the 2LiBH4-MgH2 reactive hydride composite for hydrogen storage. Metals 9(3):349. https://doi.org/10.3390/met9030349
14. Bossel, U.; Eliasson, B. Energy and the Hydrogen Economy, US DOE, EERE. Available online: https://www.afdc.energy.gov/pdfs/hyd_economy_bossel_eliasson.pdf (accessed on 15 February 2019).
15. Von Helmolt R, Eberle U (2007) Fuel cell vehicles: status 2007. J Power Sources 165(2):833–843. https://doi.org/10.1016/j.jpowsour.2006.12.073
16. Jepsen J, Bellosta von Colbe JM, Klassen T, Dornheim M (2012) Economic potential of complex hydrides compared to conventional hydrogen storage systems. Int J Hydrogen Energy 37(5):4204–4214. https://doi.org/10.1016/j.ijhydene.2011.11.141
17. Purewal J, Veenstra M, Tamburello D, Ahmed A, Matzger AJ, Wong-Foy AG, Siegel DJ (2019) Estimation of system-level hydrogen storage for metal-organic frameworks with high volumetric storage density. Int J Hydrogen Energy. https://doi.org/10.1016/j.ijhydene.2019.04.082
18. Demirocak DE, Srinivasan SS, Ram MK, Goswami DY, Stefanakos EK (2013) Volumetric hydrogen sorption measurements—Uncertainty error analysis and the importance of thermal equilibration time. Int J Hydrogen Energy 38(3):1469–1477. https://doi.org/10.1016/j.ijhydene.2012.11.013
19. Suh MP, Park HJ, Prasad TK, Lim D-W (2011) Hydrogen storage in metal-organic frameworks. Chem Rev 112(2):782–835. https://doi.org/10.1021/cr200274s
20. Thornton, Matthew J., and Simpson, Lin J. System Design, Analysis, and Modeling Activities Supporting the DOE Hydrogen Storage Engineering Center of Excellence (HSECoE): Final Project Report. United States: N. p., 2019. Web. https://doi.org/10.2172/1507683
21. Camp J, Stavila V, Allendorf MD, Prendergast D, Haranczyk M (2018) Critical factors in computational characterization of hydrogen storage in metal-organic frameworks. J Phys Chem C 122(33):18957–18967. https://doi.org/10.1021/acs.jpcc.8b04021
22. Hirscher M, Panella B, Schmitz B (2010) Metal-organic frameworks for hydrogen storage. Microporous Mesoporous Mater 129(3):335–339. https://doi.org/10.1016/j.micromeso.2009.06.005
23. Nijkamp MG, Raaymakers JEMJ, van Dillen AJ, de Jong KP (2001) Hydrogen storage using physisorption—materials demands. Appl Phys A Mater Sci Process 72(5):619–623. https://doi.org/10.1007/s003390100847
24. Frost H, Snurr RQ (2007) Design requirements for metal-organic frameworks as hydrogen storage materials. J Phys Chem C 111(50):18794–18803. https://doi.org/10.1021/jp076657p
25. Bhatia SK, Myers AL (2006) Optimum conditions for adsorptive storage. Langmuir 22(4):1688–1700. https://doi.org/10.1021/la0523816

26. Thornton AW, Simon CM, Kim J, Kwon O, Deeg KS, Konstas K, Smit B (2017) Materials genome in action: identifying the performance limits of physical hydrogen storage. Chem Mater 29(7):2844–2854. https://doi.org/10.1021/acs.chemmater.6b04933
27. Anton DL, Motyka T (2015) Hydrogen storage engineering center of excellence. United States Department of Energy, USA
28. Veenstra, M., et al. Ford/BASF-SE/UM Activities in Support of the Hydrogen Storage Engineering Center of Excellence. https://www.hydrogen.energy.gov/pdfs/review14/st010_veenstra_2014_o.pdf (United States Department of Energy, Hydrogen and Fuel Cells Program 2014 Annual Merit Review Proceedings: Project ST010, USA, 2014). Accessed 20 Nov 2019
29. Ahmed A, Seth S, Purewal J, Wong-Foy AG, Veenstra M, Matzger AJ, Siegel DJ (2019) Exceptional hydrogen storage achieved by screening nearly half a million metal-organic frameworks. Nat Commun. https://doi.org/10.1038/s41467-019-09365w
30. Ahmed A, Liu Y, Purewal J, Tran LD, Wong-Foy AG, Veenstra M, Siegel DJ (2017) Balancing gravimetric and volumetric hydrogen density in MOFs. Energy Environ Sci 10(11):2459–2471. https://doi.org/10.1039/c7ee02477k
31. Yuan D, Zhao D, Sun D, Zhou H-C (2010) An isoreticular series of metal-organic frameworks with dendritic hexacarboxylate ligands and exceptionally high gas-uptake capacity. Angew Chem Int Ed 49(31):5357–5361. https://doi.org/10.1002/anie.201001009
32. Prasad TK, Suh MP (2012) Control of interpenetration and gas-sorption properties of metal-organic frameworks by a simple change in ligand design. Chem Eur J 18(28):8673–8680. https://doi.org/10.1002/chem.201200456
33. Ahmed A, Hodgson N, Barrow M, Clowes R, Robertson CM, Steiner A, Zhang H (2014) Macroporous metal–organic framework microparticles with improved liquid phase separation. J Mater Chem A 2(24):9085–9090. https://doi.org/10.1039/c4ta00138a
34. Feng Y, Wang T, Li Y, Li J, Wu J, Wu B, Wang C (2015) Steering metallofullerene electron spin in porous metal-organic framework. J Am Chem Soc 137(47):15055–15060. https://doi.org/10.1021/jacs.5b10796
35. Wong-Ng W, Kaduk JA, Wu H, Suchomel M (2012) Synchrotron X-ray studies of metal-organic framework M 2(2,5-dihydroxyterephthalate), M = (Mn Co, Ni, Zn) (MOF74). Powder Diffr 27(04):256–262. https://doi.org/10.1017/s0885715612000863
36. Getman RB, Bae Y-S, Wilmer CE, Snurr RQ (2011) Review and analysis of molecular simulations of methane, hydrogen, and acetylene storage in metal-organic frameworks. Chem Rev 112(2):703–723. https://doi.org/10.1021/cr200217c
37. Darkrim F, Levesque D (1998) Monte Carlo simulations of hydrogen adsorption in single-walled carbon nanotubes. J Chem Phys 109(12):4981–4984. https://doi.org/10.1063/1.477109
38. Rappe AK, Casewit CJ, Colwell KS, Goddard WA, Skiff WM (1992) UFF, a full periodic table force field for molecular mechanics and molecular dynamics simulations. J Am Chem Soc 114(25):10024–10035. https://doi.org/10.1021/ja00051a040
39. Mayo SL, Olafson BD, Goddard WA (1990) DREIDING: a generic force field for molecular simulations. J Phys Chem 94(26):8897–8909. https://doi.org/10.1021/j100389a010
40. Boda D, Henderson D (2008) The effects of deviations from Lorentz-Berthelot rules on the properties of a simple mixture. Mol Phys 106(20):2367–2370. https://doi.org/10.1080/00268970802471137
41. Dubbeldam D, Calero S, Ellis DE, Snurr RQ (2016) RASPA: molecular simulation software for adsorption and diffusion in flexible nanoporous materials. Mol Simul 42(2):81–101. https://doi.org/10.1080/08927022.2015.1010082
42. Martin RL, Haranczyk M (2014) Construction and characterization of structure models of crystalline porous polymers. Cryst Growth Des 14(5):2431–2440. https://doi.org/10.1021/cg500158c
43. Panella B, Hirscher M, Roth S (2005) Hydrogen adsorption in different carbon nanostructures. Carbon 43:2209–2214
44. Gómez-Gualdrón DA, Wang TC, García-Holley P, Sawelewa RM, Argueta E, Snurr RQ, Farha OK (2017) Understanding volumetric and gravimetric hydrogen adsorption trade-off in metal-organic frameworks. ACS Appl Mater Interfaces 9(39):33419–33428. https://doi.org/10.1021/acsami.7b01190